applied sciences

MDPI

Article

Improving the Electromagnetic Vibration Energy Harvester Performance by Using a Double Coil Structure

Luigi Costanzo, Alessandro Lo Schiavo * and Massimo Vitelli

Dipartimento di Ingegneria, Università degli Studi della Campania "Luigi Vanvitelli", 81031 Aversa, Italy; luigi.costanzo@unicampania.it (L.C.); massimo.vitelli@unicampania.it (M.V.)

* Correspondence: alessandro.loschiavo@unicampania.it

Abstract: The power generation capability of an electromagnetic vibration energy harvester augmented with an additional coil was investigated and compared with that of a standard single coil electromagnetic energy harvester. A single degree of freedom model and the corresponding equivalent electric circuit were employed for the analysis of the standard and of the augmented harvesters. The harvester model was validated by means of an accurate experimental characterization of a commercial electromagnetic harvester, i.e., the model-D by ReVibe. The electric circuits for the standard and for the augmented harvesters were implemented by electronic components and experimentally tested to determine the maximum power they are able to generate in four test conditions. Results from simulations and from experiments showed significant improvement of the power extraction performance exhibited by the double coil energy harvester, particularly at frequencies lower than the harvester mechanical resonance frequency.

Keywords: energy harvester; electronic optimization circuit; micro power generators; Internet of Things device's supply

Citation: Costanzo, L.; Lo Schiavo, A.; Vitelli, M. Improving the Electromagnetic Vibration Energy Harvester Performance by Using a Double Coil Structure. *Appl. Sci.* **2022**, *12*, 1166. https://doi.org/10.3390/app12031166

Academic Editors: Adel Razek and Alfio Dario Grasso

Received: 16 December 2021
Accepted: 20 January 2022
Published: 23 January 2022

1. Introduction

Internet of Things (IoT) devices are an effective, sustainable, and cheap solution for implementing wireless sensor networks and for the monitoring of transportation vehicles, of industrial implants (Industry 4.0), of the environment and of smart cities [1]. Such devices are frequently employed in places or infrastructure where a wired energy supply is not present, or its distribution is not economically convenient. In these cases, a solution for the energy supply of IoT devices is represented by disposable batteries which, however, are characterised by high maintenance costs, high environmental impact and low reliability. An alternative solution is represented by energy harvesting systems [2,3] that are able to convert into electricity otherwise wasted forms of energy, without suffering from the problems of disposable batteries [4]. For this reason, energy harvesting systems have found application in very different fields such as, for example, trains [5], backpacks [6], tiles [7], logistics, construction, mining, aviation, military and industry 4.0 [8,9].

Among the energy harvesting systems, resonant vibration harvesters, which are able to convert into electricity the mechanical energy from ambient vibrations, are particularly attractive due to the wide availability of vibrations into the environment. These harvesters usually exploit a piezoelectric material or the electromagnetic effect [10,11]. Resonant electromagnetic harvesters are able to generate higher power with respect to resonant piezoelectric harvesters even if, like resonant piezoelectric harvesters, they are able to efficiently operate only when the vibration frequency is near to their resonance frequency. Unfortunately, in most practical cases, the ambient vibrations are frequency-varying or exhibit a random behavior with an energy content that is distributed over a wide frequency spectrum [12].

For these reasons, many research efforts have been made to increase the energy efficiency of resonant electromagnetic harvesters by resorting to harvester arrays [13,14],

non-linear harvesters [15,16], and various electrical or mechanical tuning techniques [17]. Electrical tuning techniques aim to match the harvester with its optimal load impedance, frequency by frequency, by using properly controlled active power electronic circuits according to the maximum power transfer theorem [18,19]. Mechanical tuning techniques attempt to regulate some mechanical parameters to adapt the resonance frequency to the vibration frequency [20]. In particular, the resonance frequency of the device can be adjusted by rotating a spring [21], or by exploiting a magnetorheological elastomer [22], a magnetic force [23,24] or a suitable actuator [25,26]. Among the tuning techniques, the idea presented in [27] and based on a double coil electromagnetic harvester seems very attractive for its potential.

Thus, in this paper the performance of a resonant electromagnetic energy harvester characterized by a double coil is investigated and the power extraction capabilities of this harvester are compared with those of a standard single coil resonant electromagnetic harvester. The latter device exploits the time-varying relative displacement between a magnet and a coil caused by the ambient vibrations to generate electrical energy. On the other hand, a double coil electromagnetic energy harvester is equipped with an additional coil, which is electromagnetically coupled with the magnet and is in relative motion with respect to both the magnet and the primary coil.

Here, the double coil electromagnetic harvester was modeled as a single degree of freedom system and its equivalent electric circuit was exploited to predict by simulations the maximum power that the harvester was able to generate. Moreover, experimental tests were performed on a commercial single coil electromagnetic harvester, the model-D by ReVibe, in order to characterize its behavior and to extract the parameters of its single degree of freedom model. Such a model was used to implement the equivalent electric circuits of both a single coil and of a double coil harvester, by using electronic components mounted on a solder-less breadboard. Then, experimental tests were performed in order to compare the power delivered to their optimal loads by the two types of harvester. Test results showed that the double coil harvester was able to significantly increase the power efficiency at frequencies lower than the mechanical resonance frequency.

2. Double Coil Electromagnetic Harvester

In order to predict the maximum power that can be extracted by a standard single coil harvester and by a double coil electromagnetic harvester, the single degree of freedom models of both harvesters are presented here. Firstly, the single coil electromagnetic harvester is studied and then the double coil harvester is analyzed.

A standard single coil electromagnetic harvester is made up of a vibrating case which houses a permanent magnet linked to a spring system and a coil fixed to the housing and connected to the electrical load, as shown in Figure 1. When a vibration is applied to the case, the spring system makes the permanent magnet moving out of phase with respect to the coil and the relative displacement between the magnet and the coil leads to the conversion of mechanical energy into electrical energy.

During its movement, the permanent magnet is subject to the viscous damping force of the medium, to the elastic force of the spring and to the electromagnetic (Lorentz) force due to the interaction between the current flowing into the coil and the induction field of the magnet. If a single degree of freedom model is employed for the sake of simplicity, Newton's second law can be written as [28]

$$m\,\ddot{x}(t) + c\,\dot{x}(t) + k_s\,x(t) + \theta\,i_{LOAD}(t) = -m\,\ddot{y}(t) \tag{1}$$

where $\ddot{y}(t)$ denotes the acceleration of the case, $x(t)$ the relative displacement between the magnet and the coil, m the magnet mass, c the viscous damping coefficient, k_s the equivalent stiffness of the spring system, and $i_{LOAD}(t)$ the electrical current flowing into the coil. θ is the electromechanical coupling coefficient of the coil that takes into account its

geometrical properties, its number of turns and the magnetic field strength, as shown in detail in [28]. This current is due to the electromotive force (e.m.f.) induced in the coil:

$$\varepsilon(t) = \theta\, \dot{x}(t) \tag{2}$$

and flows through the coil resistance and inductance as well as through the electrical load connected to the coil. Equations (1) and (2) can be represented by the equivalent electric circuit shown in Figure 2, where $k = m/\theta$, $R_m = \theta^2/c$, $L_m = \theta^2/k_s$, $C_m = m/\theta^2$, being R_C and L_C the resistance and the inductance of the coil, respectively [17].

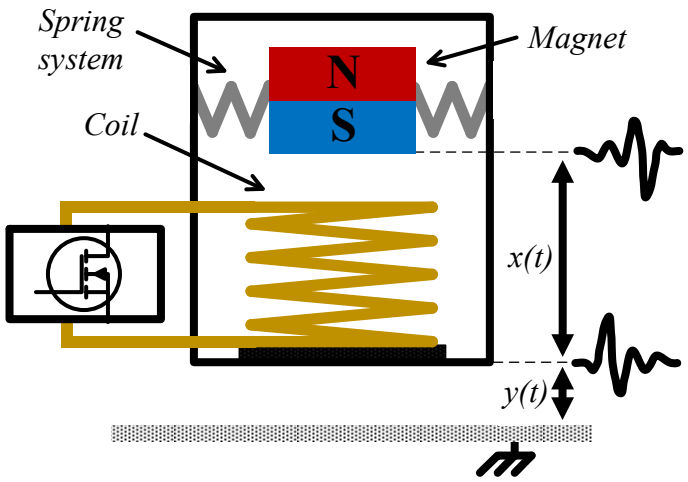

Figure 1. Schematic representation of a standard single coil resonant electromagnetic vibration energy harvester.

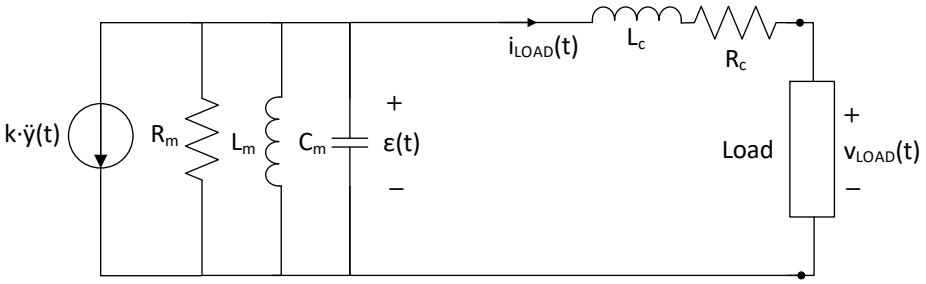

Figure 2. Equivalent circuit of a standard single coil resonant electromagnetic vibration energy harvester.

When the single coil electromagnetic harvester is driven by a sinusoidal vibration at frequency $\omega_{VIB} = 2\,\pi\, f_{VIB}$, i.e., $\ddot{y}(t) = A_{VIB}\sin(2\,\pi\, f_{VIB}\, t)$, the average power that can be delivered to the load can be predicted by applying the phasor method to the equivalent circuit in Figure 2, i.e.,

$$P_{LOAD} = \frac{\left|\bar{I}_{LOAD}\right|^2}{2}\cdot R_{LOAD} \tag{3}$$

where $\bar{I}_{LOAD}$ is the phasor of the load current $i_{LOAD}(t)$ and R_{LOAD} is the resistive part of the load. According to the maximum power transfer theorem, the maximum average power is delivered to the load when its impedance is equal to the complex conjugate of the source impedance, i.e., $\dot{Z}_{LOAD} = \dot{Z}_{OPT} = R_{OPT} + j\cdot X_{OPT}$ where,

$$R_{OPT}(\omega_{VIB}) = \frac{\theta^2\cdot\omega_{VIB}^2\cdot c}{\left(k_s - m\cdot\omega_{VIB}^2\right)^2 + \left(\omega_{VIB}\cdot c\right)^2} + R_c \tag{4}$$

$$X_{OPT}(\omega_{VIB}) = \frac{\theta^2 \cdot \omega_{VIB} \cdot (m \cdot \omega_{VIB}^2 - k_s)}{(k_s - m \cdot \omega_{VIB}^2)^2 + (\omega_{VIB} \cdot c)^2} - X_c(\omega_{VIB}) \quad (5)$$

being $X_c(\omega_{VIB}) = \omega_{VIB}\, L_C$. When the load is equal to that in (4) and (5), the extracted power in (3) becomes:

$$P_{OPT}(\omega_{VIB}) = P_{LOAD}(R_{OPT}, X_{OPT}, \omega_{VIB}) = \frac{1}{8} \cdot \frac{A_{VIB}^2 \cdot m^2 \cdot \omega_{VIB}^2 \cdot \theta^2}{R_c \cdot \left[(k_s - m \cdot \omega_{VIB}^2)^2 + (\omega_{VIB} \cdot c)^2 \right] + c \cdot (\omega_{VIB} \cdot \theta)^2} \quad (6)$$

Equation (6) shows that the harvester exhibits a resonant behavior, characterized by the resonance frequency f_{RES} and the angular frequency ω_{RES} given by:

$$\omega_{\mathrm{RES}} = 2 \cdot \pi \cdot f_{\mathrm{RES}} = \sqrt{\frac{k_s}{m}} \quad (7)$$

At f_{RES} the harvester supplies the maximum power P_{MAX} to the optimal load

$$P_{MAX} = P_{OPT}(\omega_{RES}) = \frac{1}{8} \cdot \frac{A_{VIB}^2 \cdot m^2 \cdot \theta^2}{R_c \cdot c^2 + c \cdot \theta^2} \quad (8)$$

A typical trend of the average power delivered to the optimal load is shown in Figure 3.

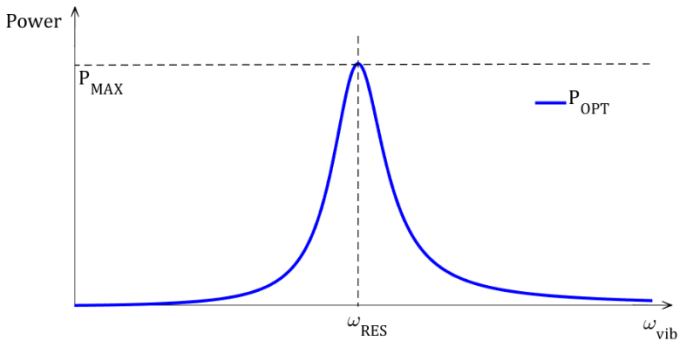

Figure 3. Typical trend of the maximum average power, P_{OPT}, as a function of the vibration frequency, ω_{VIB}, according to Equation (6), for a standard single coil electromagnetic harvester.

In a double coil electromagnetic harvester, shown in Figure 4a, an additional second coil, which is rigidly connected to the fixed reference frame of the first coil, is added to a standard single coil electromagnetic harvester. The additional second coil is electrically connected to an additional electrical load. In practical applications, both the load of the first coil and the load of the second coil are implemented through ac/dc converters to transform the ac output voltage into a dc voltage used to supply a storage system, which can be a rechargeable battery or a supercapacitor. Note that for a double coil electromagnetic harvester, the storage system is the same for the two loads, so that the effective power extracted by the harvester is the sum of the power extracted by the first coil and of the power extracted by the second coil. An example of a possible installation of the double coil harvester on a freight wagon, which as known does not have a power supply from the locomotive or from the overhead power line, is shown in Figure 4b. The first coil (positioned at the bottom of Figure 4a) is rigidly connected to the vibrating chassis of the bogie (positioned at the top of Figure 4b) and the second coil (positioned at the top of Figure 4a) is rigidly connected to the frame of the wheel axles (positioned at the bottom of Figure 4b).

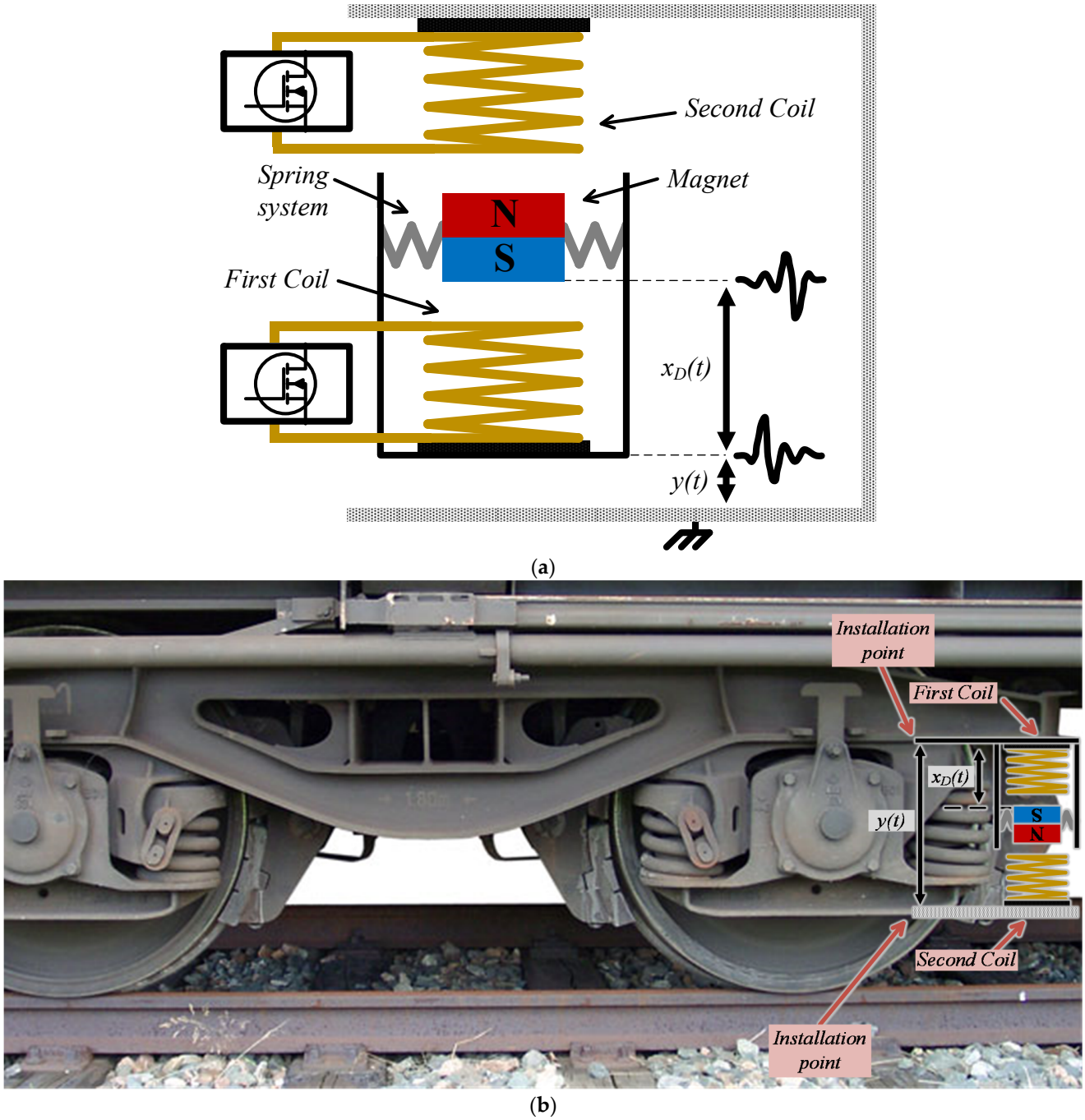

Figure 4. (**a**) Schematic representation of a double coil resonant electromagnetic vibration energy harvester. (**b**) Possible installation on a fright wagon.

In the double coil electromagnetic harvester, the permanent magnet is subject to an additional electromagnetic force due to the second coil. Thus, Newton's second law in Equation (1) can be now written as

$$m\,\ddot{x}_D(t) + c\,\dot{x}_D(t) + k_s\,x_D(t) + \theta_1\,i_{LOAD\_1}(t) + \theta_2\,i_{LOAD\_2}(t) = -m\,\ddot{y}(t) \tag{9}$$

where $x_D(t)$ is the relative displacement between the magnet and the first coil in the double coil harvester, $i_{LOAD\_1}(t)$ and $i_{LOAD\_2}(t)$ are the electrical currents flowing into the first and the second coil, respectively. θ_1 and θ_2 are the electromechanical coupling coefficients of the first and of the second coil respectively, which depend on their geometric properties,

their number of turns and the magnetic field strength [28]. Note that, in the double coil harvester, the relative displacement between the magnet and the second coil is $x_D(t) + y(t)$. Therefore, the electromotive forces (e.m.f.) induced in the two coils can be written as:

$$\varepsilon_1(t) = \theta_1 \, \dot{x}_D(t) \tag{10}$$

$$\varepsilon_2(t) = \theta_2 \left[\dot{x}_D(t) + \dot{y}(t)\right] = \frac{\theta_2}{\theta_1}\varepsilon_1(t) + \theta_2 \, \dot{y}(t) \tag{11}$$

If, without any loss of generality, a second additional coil with the same parameters as the first coil (same coil resistance $R_{c2} = R_{c1}$, same coil inductance $L_{c2} = L_{c1}$ and same electromechanical coupling coefficient $\theta_2 = \theta_1 = \theta$) is considered, according to Equations (9)–(11) the double coil electromagnetic harvester can be modeled by the equivalent electric circuit in Figure 5. By exploiting the equivalent circuit in Figure 5, it is possible to calculate the average power delivered to the load connected to the first coil, P_{LOAD_1}, and the power delivered to the load connected to the second coil, P_{LOAD_2}. These two powers depend on both the loads connected to the first and to the second coil, and their maximum values, which depend on the vibration frequency, will be called in the following P_{OPT_1} and P_{OPT_2}.

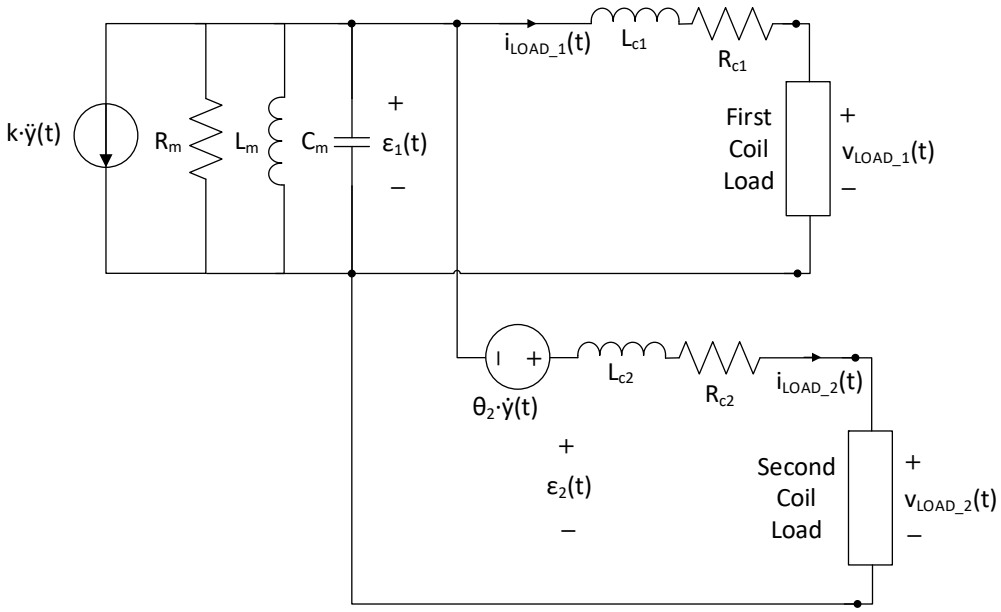

Figure 5. Equivalent circuit of a double coil resonant electromagnetic vibration energy harvester whose second additional coil has the same parameters of the first coil ($R_{c2} = R_{c1}$, $L_{c2} = L_{c1}$ and $\theta_2 = \theta_1 = \theta$.

It is interesting to observe that the presence of the voltage generator $\theta_2 \, \dot{y}(t)$ is the key difference between the standard single coil electromagnetic harvester and the considered double coil electromagnetic harvester. Thanks to the presence of such a voltage generator $\theta_2 \, \dot{y}(t)$, the sum of the maximum average powers delivered to the two loads, $P_{OPT\_1} + P_{OPT\_2}$, can exceed the power delivered to the load of a single coil electromagnetic harvester, P_{OPT}. Therefore, it is possible to define the power gain due to the additional coil as a function of the frequency displacement from the resonance frequency $\Delta f = (f_{VIB} - f_{RES})/f_{RES}$ as:

$$\eta_P(\Delta f) = \frac{P_{OPT\_1}(\Delta f) + P_{OPT\_2}(\Delta f)}{P_{OPT}(\Delta f)} \tag{12}$$

Simulation and experimental results reported in Section 4 show that the power gain can be significantly greater than 1.

3. Commercial Harvester Characterization

A commercial single coil electromagnetic energy harvester was characterized to obtain the parameters of its equivalent circuit, which will be used in the next Section to perform simulations and experimental tests.

The photo and the block diagram of the experimental setup employed for the harvester characterization are shown in Figure 6a,b, respectively. In particular, the electromagnetic harvester model-D by ReVibe, the photo of which is shown in Figure 6c and the technical parameters reported in Figure 6d, is mounted on the shaker Sentek VT-500. The driving current of the shaker is generated by the LA-800 Power Amplifier and the driving signal of the power amplifier is provided by the controller Spider-81 by Crystal Instruments that implements the closed loop vibration control by measuring the acceleration of the vibration generated by the shaker.

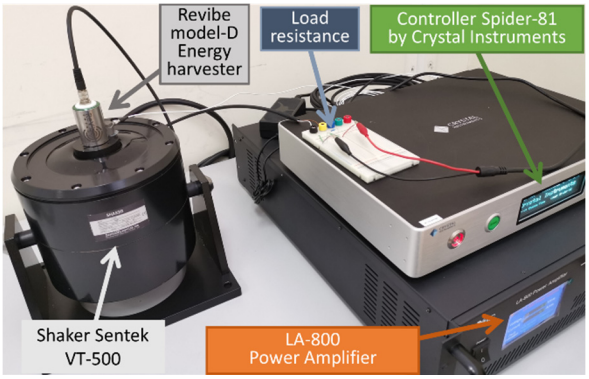

(**a**)

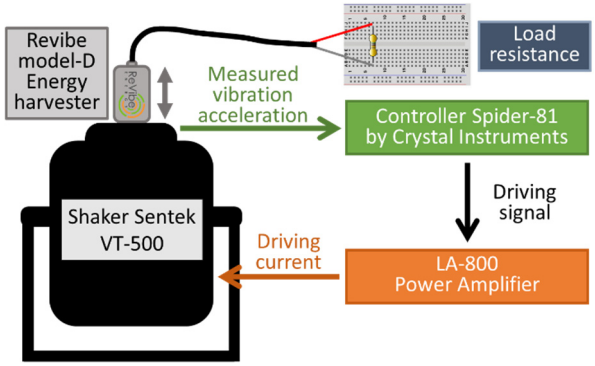

(**b**)

(**c**)

Model	ModelD v.5 Harvester
Part Number	00202
Serial Number	040173 & 040174
Target Frequency	100 Hz (±1Hz)
Dimensions	H 57.5 mm Ø33mm
Casing Material	Stainless steel
Weight	135 g
Output	Unregulated AC
Reference electrical load	1000 Ohm
Connector type	Binder connector (included)

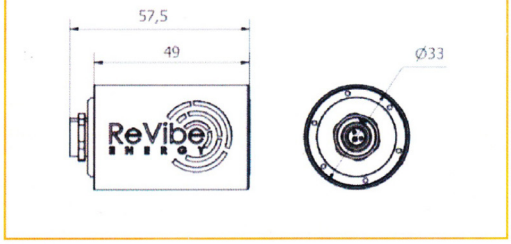

(**d**)

Figure 6. (**a**) Characterization setup for the electromagnetic energy harvester model-D by ReVibe. (**b**) Block diagram of the characterization setup. (**c**) Photo of the harvester. (**d**) Technical parameters of the harvester as reported in the datasheet.

To test the open circuit behavior of the considered electromagnetic harvester, a sinusoidal vibration having a constant acceleration equal to $A_{VIB} = 1$ g and a varying frequency was applied to the harvester with open output terminals. The measured amplitude of the open-circuit voltage $v_{OC}(t)$ is reported in Figure 7a.

Moreover, to test the behavior of the harvester feeding different resistive loads, a sinusoidal vibration with a constant acceleration equal to $A_{VIB} = 1$ g and a varying frequency was applied to the harvester with the output terminals connected to different load resistors, i.e., $R_{LOAD} = 1200\ \Omega$, $R_{LOAD} = 1000\ \Omega$ and $R_{LOAD} = 820\ \Omega$. The measured voltage amplitudes and the measured average powers delivered to the loads are reported in Figure 7b,c, respectively, and are in line with data declared by the harvester manufacturer [8].

The above measurements allowed us to deduce that the mechanical resonance frequency, i.e., the frequency at which the open-circuit voltage reaches the maximum amplitude value, is equal to $f_{RES} = 98.5$ Hz. Moreover, they allowed us to determine the amplitude of the open-circuit voltage at the resonance frequency, $V_{OC\_MAX}(1\text{ g}) = 19.9$ V, the open-circuit 3-dB

bandwidth, $B_{3dB} = 2.6$ Hz and the optimal load resistance, $R_{LOAD\_MAX} = 1000\ \Omega$, which is the resistance that allows the maximum average power extraction at the resonance frequency.

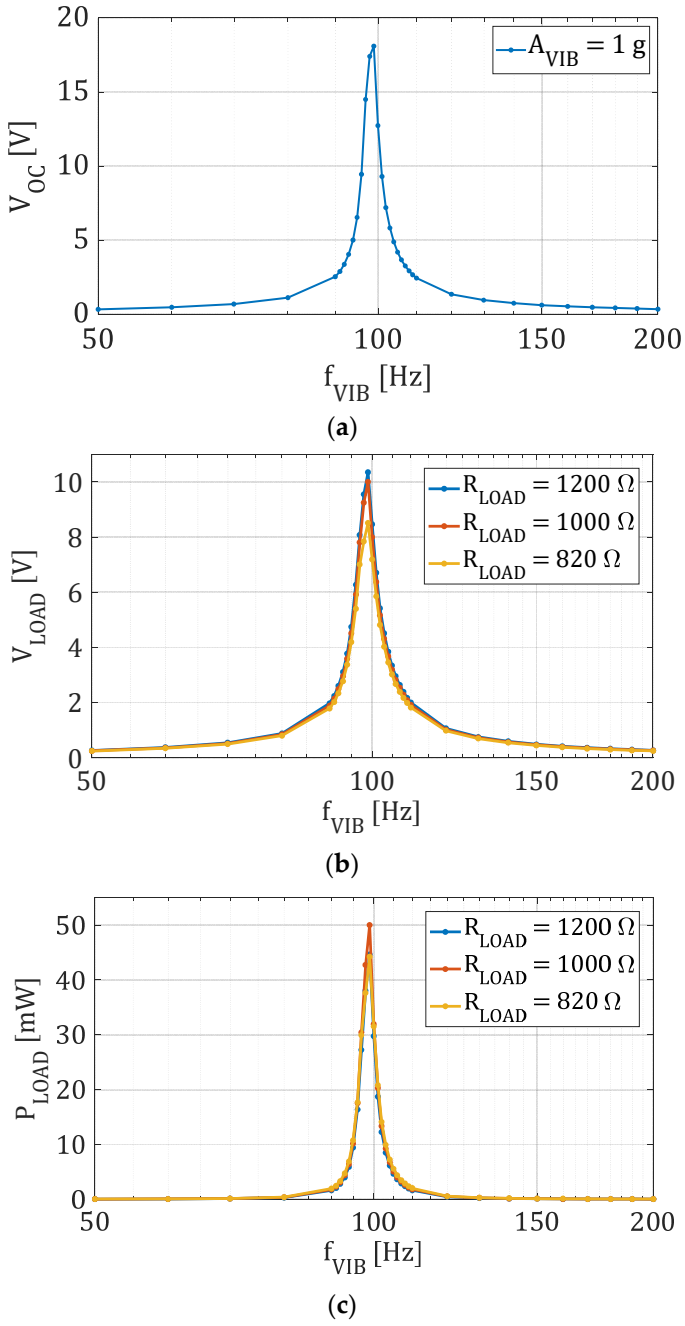

Figure 7. Measurements carried out on the commercial harvester model-D by ReVibe. (**a**) Open-circuit voltage amplitude; (**b**) output voltage amplitude for different loads; (**c**) extracted average power for different loads.

The resistance and the inductance of the coil of the considered electromagnetic harvester were measured by using the LCR Meter U1733C by Keysight Technologies. It resulted as $R_C = 300\ \Omega$ and $L_C = 135$ mH.

By exploiting the above measurements, the parameters of the equivalent circuit of the single coil electromagnetic harvester model-D by ReVibe were deduced. In detail, from the analytical expression of the optimal load resistance obtained by the maximum power transfer theorem,

$$R_{LOAD\_MAX} = \sqrt{(R_m + R_c)^2 + (2\pi f_{RES} \cdot L_c)^2} \tag{13}$$

it was possible to calculate $R_m = 700\ \Omega$. From the expression of the maximum open-circuit voltage amplitude at the resonance frequency under 1 g acceleration,

$$V_{OC\_MAX} = k \cdot A_{VIB} \cdot R_m \tag{14}$$

it was deduced that $k = 28$ mA/g. From the open-circuit 3 dB bandwidth,

$$B_{3dB} = \frac{1}{R_m \cdot C_m} \tag{15}$$

the capacitance value $C_m = 87.5$ µF was obtained. Finally, from the expression of the resonance frequency f_{RES}

$$f_{RES} = \frac{1}{2 \cdot \pi \cdot \sqrt{L_m \cdot C_m}} \tag{16}$$

it was calculated that $L_m = 29.9$ mH. All the parameters of the equivalent circuit of the considered electromagnetic harvester are summarized in Table 1.

Table 1. Parameters of the equivalent circuit of the tested commercial electromagnetic harvester.

Parameter	Value
k	28 mA/g
R_m	700 Ω
L_m	29.9 mH
C_m	87.5 µF
R_c	300 Ω
L_c	135 mH

To validate the accuracy of the equivalent circuit in emulating the behavior of the considered commercial harvester, the equivalent circuit was implemented by using electronic components mounted on a solderless breadboard, in the Thevenin alternative form shown in Figure 8 that is equivalent to that in Figure 2. The inductance L_m was implemented through an active circuit based on operational amplifiers, i.e., the Antoniou inductance-simulation circuit. By using the automatic measurement option of the oscilloscope DSOX1204G-D1200BW1A by Keysight Technology the transfer function $G_{CIRCUIT}(f_{VIB}) = V_P/V_G$ was obtained for $R_{LOAD} = 1000\ \Omega$, as shown in Figure 9a. V_P and V_G are the voltages with respect to ground of points P and G, respectively (Figure 8). $G_{CIRCUIT}(f_{VIB})$ can be expressed as a function of the complex quantities V_{OC} and V_{LOAD}, previously measured on the commercial harvester (Figure 7):

$$G_{CIRCUIT}(f_{VIB}) = \frac{V_P}{V_G} = \frac{V_{OC} - V_{LOAD}}{V_{OC}} = 1 - \frac{V_{LOAD}}{V_{OC}} \tag{17}$$

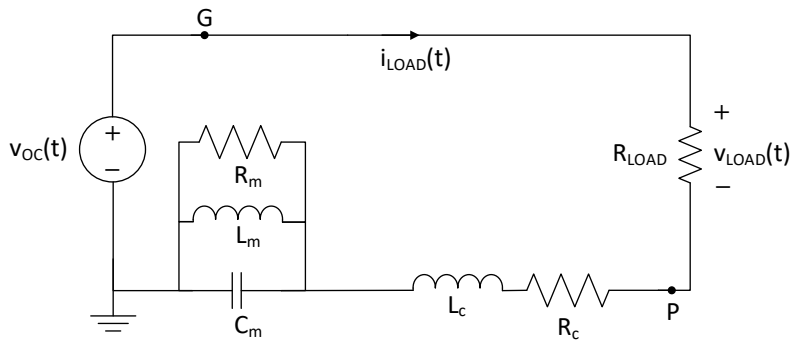

Figure 8. Alternative Thevenin form of the equivalent circuit of a single coil resonant electromagnetic vibration energy harvester.

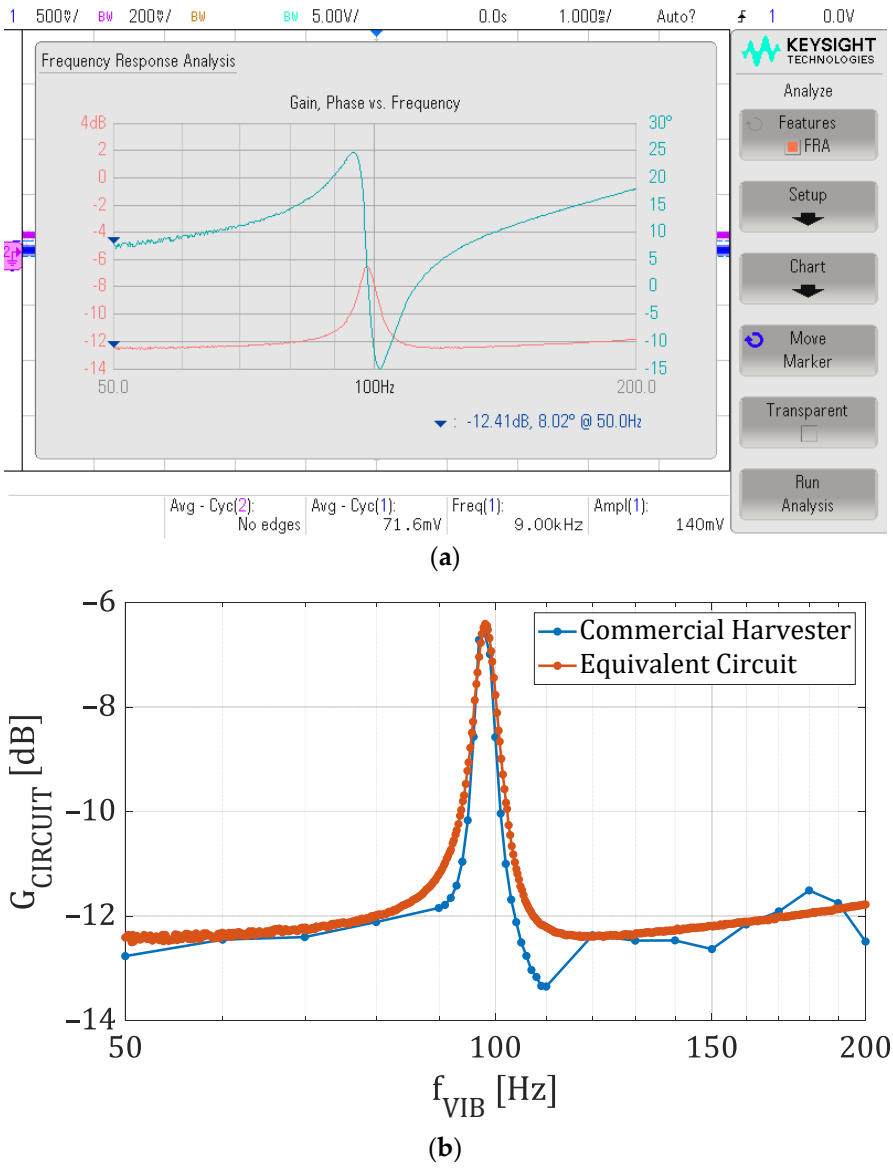

Figure 9. Comparison of measurements performed on the considered commercial harvester and on its equivalent circuit. (**a**) Oscilloscope screenshot of the gain and phase of the transfer function $G_{CIRCUIT}$ of the equivalent circuit. (**b**) Transfer functions $G_{CIRCUIT}$ measured on the commercial harvester and on the implemented equivalent circuit.

Therefore, the transfer function $G_{CIRCUIT}(f_{VIB})$ measured on the implemented equivalent circuit and that calculated by using the measurements on the commercial harvester were compared, as shown in Figure 9b. The comparison shows a very good agreement of the electrical behaviors of the commercial harvester and of the equivalent circuit.

4. Simulation and Experimental Results

Simulations and experimental tests were performed to show that the double coil electromagnetic harvester is able to deliver an amount of energy significantly greater than that provided by a standard single coil electromagnetic harvester.

Firstly, numerical simulations of the circuit of the single coil harvester shown in Figure 2 and of the circuit of the double coil harvester shown in Figure 5 were performed. The parameters used for the single coil harvester are those obtained by the experimental characterization of the commercial harvester reported in the previous section. The parameters used for the double coil harvester are the same as for the single coil harvester with the

addition of $R_{c2} = R_{c1} = R_c$, $L_{c2} = L_{c1} = L_c$ and $\theta_2 = \theta_1 = \theta$. For each value of the vibration frequency, the load of the single coil harvester was varied to determine the optimal load that allows the maximum power extraction $P_{OPT} = \max(P_{LOAD})$. Also, the values of the loads of the double coil harvester were varied to determine the optimal loads that allow the maximization of the total extracted power $P_{OPT\_D} = \max(P_{LOAD1} + P_{LOAD2}) = P_{OPT1} + P_{OPT2}$. Then, the performance improvement of the double coil harvester was calculated as the power gain $\eta_P(\Delta f)$ in (12).

The power gain obtained by numerical simulations and reported in Figure 10 shows that an increase of the extracted power is obtained by using the double coil harvester for any vibration frequency. Moreover, this increase is particularly significant for frequencies lower and far from the resonance frequency.

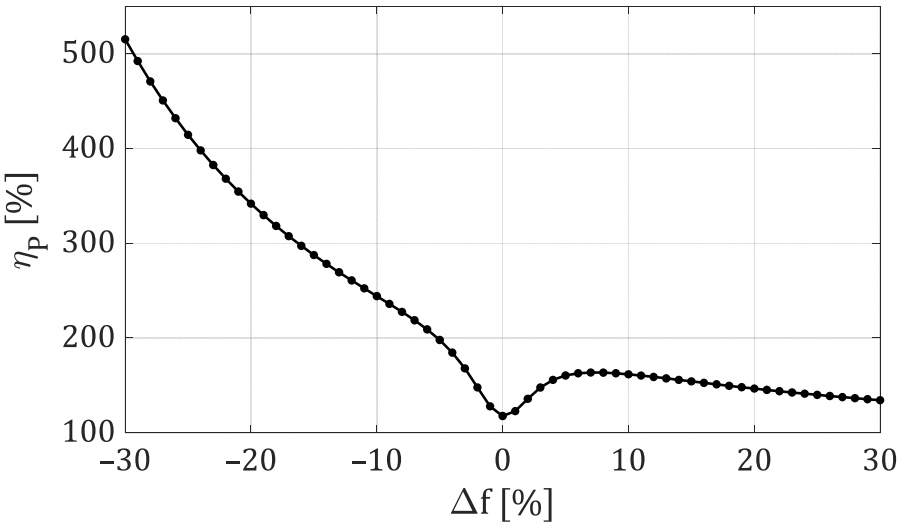

Figure 10. Power gain η_P of the double coil harvester with respect to the single coil harvester, as a function of the frequency displacement from the resonance frequency Δf.

Experimental tests were performed on the electrical circuit of a single coil harvester reported in Figure 8 and on the electrical circuit of a double coil harvester reported in Figure 11a. These circuits were implemented by using electronic components mounted on a solderless breadboard as shown in Figure 11b. It should be emphasized that the experimental tests were performed on the equivalent circuits of the harvesters and not on the harvesters themselves because a double coil harvester has never been built up. Therefore, before constructing a double coil harvester, it seems useful to preliminarily investigate its potential.

Tests were performed for four case studies, which differ for the vibration frequency ($f_{VIB} = 0.9\ f_{RES}$, $f_{VIB} = 0.8\ f_{RES}$, $f_{VIB} = 0.7\ f_{RES}$) and for the acceleration amplitude ($A_{VIB} = 1$ g, $A_{VIB} = 2$ g), as detailed in Table 2.

For each of the four test cases, for the single coil harvester the values of the load resistance R_{LOAD} and of the load capacitance C_{LOAD} were varied to determine the optimal values, R_{LOAD_OPT} and C_{LOAD_OPT}, that ensure the maximum average power extraction, P_{OPT}. It is worth noting that only ohmic-capacitive loads were considered since, at the working frequency f_{VIB} (lower than f_{RES}), in all the considered test cases the equivalent harvester impedance was always ohmic-inductive. The phase relationships of the voltages, currents and power, measured in the first test case in the optimal condition, and reported in Figure 12a,b, confirm the ohmic-capacitive nature of the optimal load. For all the four test cases, the trends of the measured average load power of the single coil circuit are reported in Figure 13 as a function of the load resistance R_{LOAD} and of the load capacitance C_{LOAD}. The optimal values of R_{LOAD} and C_{LOAD} for each test case are summarized in Table 2, together with the maximum extracted power P_{OPT}.

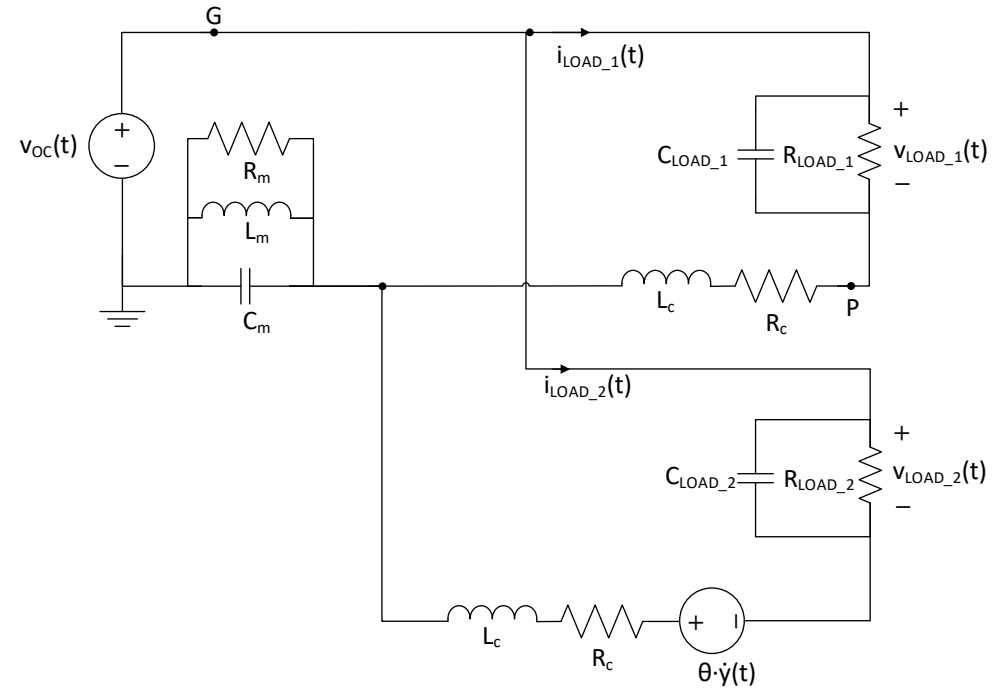

(**a**)

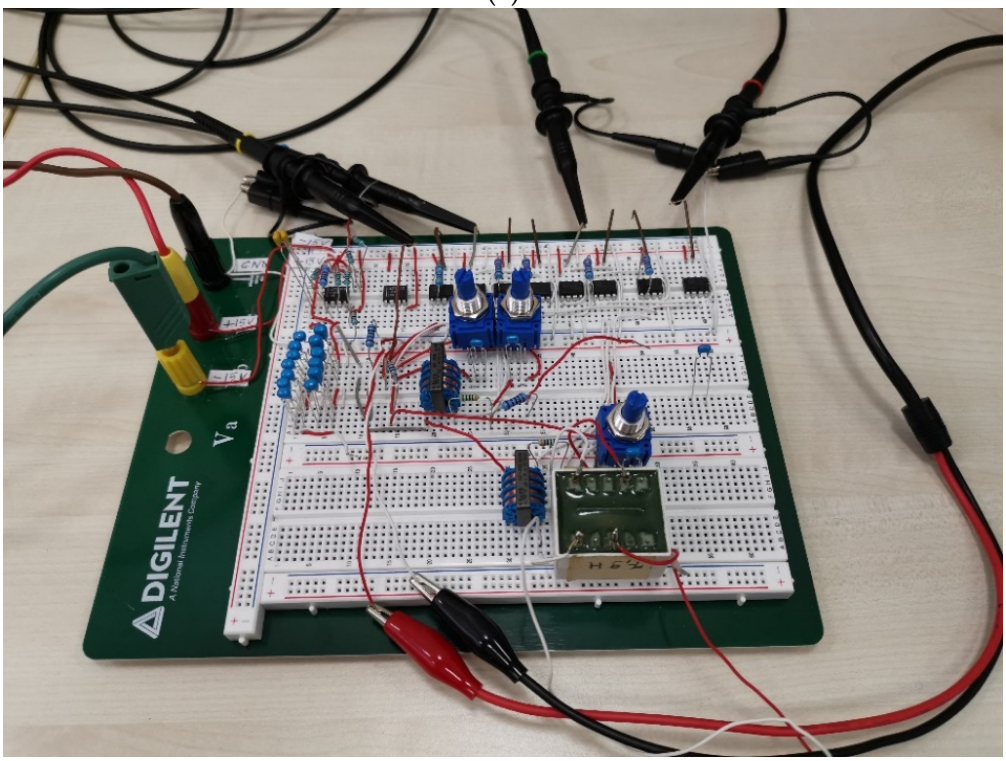

(**b**)

Figure 11. (**a**) Alternative form of the equivalent circuit of a double coil electromagnetic harvester. (**b**) Experimental implementation of the electromagnetic harvesters by using electronic components.

Table 2. Experimental tests on the electrical circuits of single coil and double coil harvesters.

Test Case		n. 1	n. 2	n. 3	n. 4
Test conditions	Δf	−10%	−20%	−20%	−30%
	f_{VIB}	0.9·f_{RES}	0.8·f_{RES}	0.8·f_{RES}	0.7·f_{RES}
	A_{VIB}	1 g	1 g	2 g	2 g
Single coil harvester	R_{LOAD_OPT}	388 Ω	388 Ω	388 Ω	388 Ω
	C_{LOAD_OPT}	1 µ	1 µ	1 µ	1 µ
	P_{OPT}	**2.36 mW**	**0.56 mW**	**2.19 mW**	**0.84 mW**
Double coil harvester	$R_{LOAD\_1\_OPT}$	558 Ω	558 Ω	558 Ω	558 Ω
	$C_{LOAD\_1\_OPT}$	1 µ	1 µ	1 µ	1 µ
	P_{OPT_1}	2.16 mW	0.53 mW	2.19 mW	0.79 mW
	$R_{LOAD\_2\_OPT}$	558 Ω	558 Ω	558 Ω	558 Ω
	$C_{LOAD\_2\_OPT}$	1 µ	1 µ	1 µ	1 µ
	P_{OPT_2}	3.14 mW	1.19 mW	5.03 mW	3.33 mW
	$P_{OPT\_D} = P_{OPT\_1} + P_{OPT\_2}$	**5.3 mW**	**1.72 mW**	**7.22 mW**	**4.12 mW**
Power Gain $\eta = P_{OPT\_D}/P_{OPT}$	Experiments	224%	307%	330%	490%
	Simulations	244%	342%	342%	515%

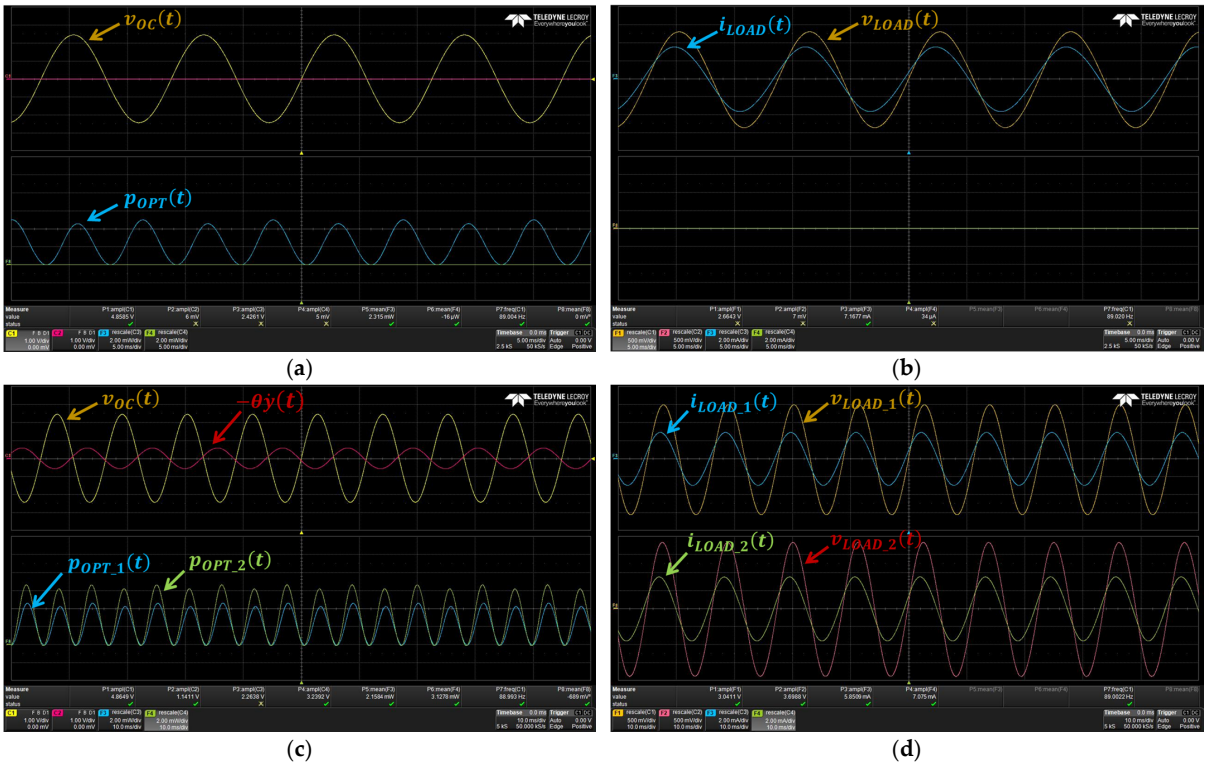

Figure 12. Oscilloscope screenshots obtained in the optimal conditions for the first test case. Test for the single coil circuit in Figure 8: (**a**), input voltage $v_{OC}(t)$ (yellow line) and instantaneous load power $p_{OPT}(t)$ (blue line); (**b**) load voltage $v_{LOAD}(t)$ (yellow line) and load current $i_{LOAD}(t)$ (blue line). Test for the double coil circuit in Figure 11a: (**c**) input voltage $v_{OC}(t)$ (yellow line), additional voltage $\theta\dot{y}(t)$ (red line), instantaneous power on the first load $p_{OPT\_1}(t)$ (blue line), and instantaneous power on the second load $p_{OPT\_2}(t)$ (green line); (**d**) first load voltage $v_{LOAD\_1}(t)$ (yellow line), first load current $i_{LOAD\_1}(t)$ (blue line), second load voltage $v_{LOAD\_2}(t)$ (red line), and second load curren $i_{LOAD\_2}(t)$ (green line).

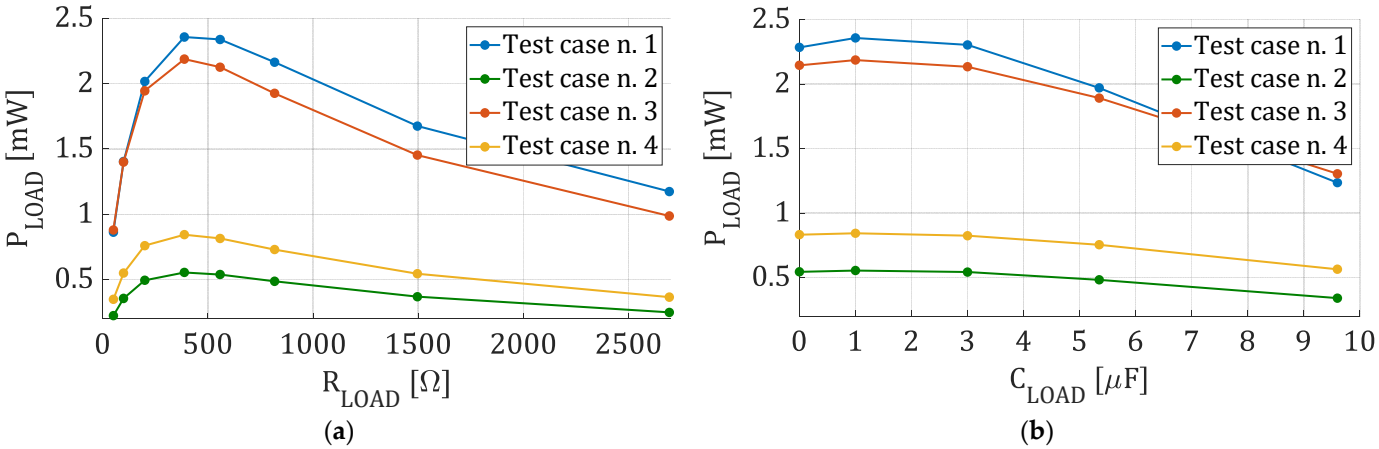

Figure 13. Measured average load power for the single coil circuit in Figure 8, in the four test cases. (**a**) Power as a function of the load resistance for the optimal load capacitance. (**b**) Power as a function of the load capacitance for the optimal load resistance.

Moreover, for each of the four test cases, for the double coil harvester the values of the first load resistance R_{LOAD_1}, the first load capacitance C_{LOAD_1}, the second load resistance R_{LOAD_2}, and the second load capacitance C_{LOAD_2} were varied to determine the optimal values that ensure the maximum power extraction, $P_{OPT\_D} = \max(P_{LOAD\_1} + P_{LOAD\_2})$. For the first test case, oscilloscope screenshots of the voltages, currents and power measured in the optimal condition of the double coil harvester are reported in Figure 12c,d. For all the four test cases, the trends of the measured average load power of the double coil circuit are reported in Figure 14 as a function of the load resistances and load capacitances. The optimal values of the load resistances and capacitances for each test case are summarized in Table 2, together with the maximum average extracted powers.

Starting from the maximum average powers extracted from the single coil harvester and from the double coil harvester in each test case, it is possible to calculate the power gain $\eta_P = P_{OPT\_D}/P_{OPT}$, i.e., the performance improvement for the double coil harvester. Experimental values for the power gain are reported in Table 2, together with the corresponding values obtained by the simulations reported in Figure 10. Experimental tests confirm the simulations' results and validate the performance improvement that the double coil harvester can provide.

Finally, note that an increase in the extracted power can also be obtained by increasing the number of turns of the single coil standard harvester. In particular, if the number of turns is doubled (e.g., by inserting the additional coil, equal to the first coil, in series with it) the electromechanical coupling coefficient θ and the electrical equivalent resistance R_c of the resulting coil are doubled. Therefore, according to Equation (6), the extracted power P_{SERIES} with the two series-connected coils is confined between once and twice that (P_{OPT}) of the original standard harvester. In particular, for small values of R_c, P_{SERIES} tends to P_{OPT}; for large values of R_c, P_{SERIES} tends to twice P_{OPT}. On the other hand, the double coil harvester investigated here is able to extract a power greater than twice P_{OPT}, as shown in Table 2. In particular, the power gain can be about five times greater than that of a standard single coil harvester.

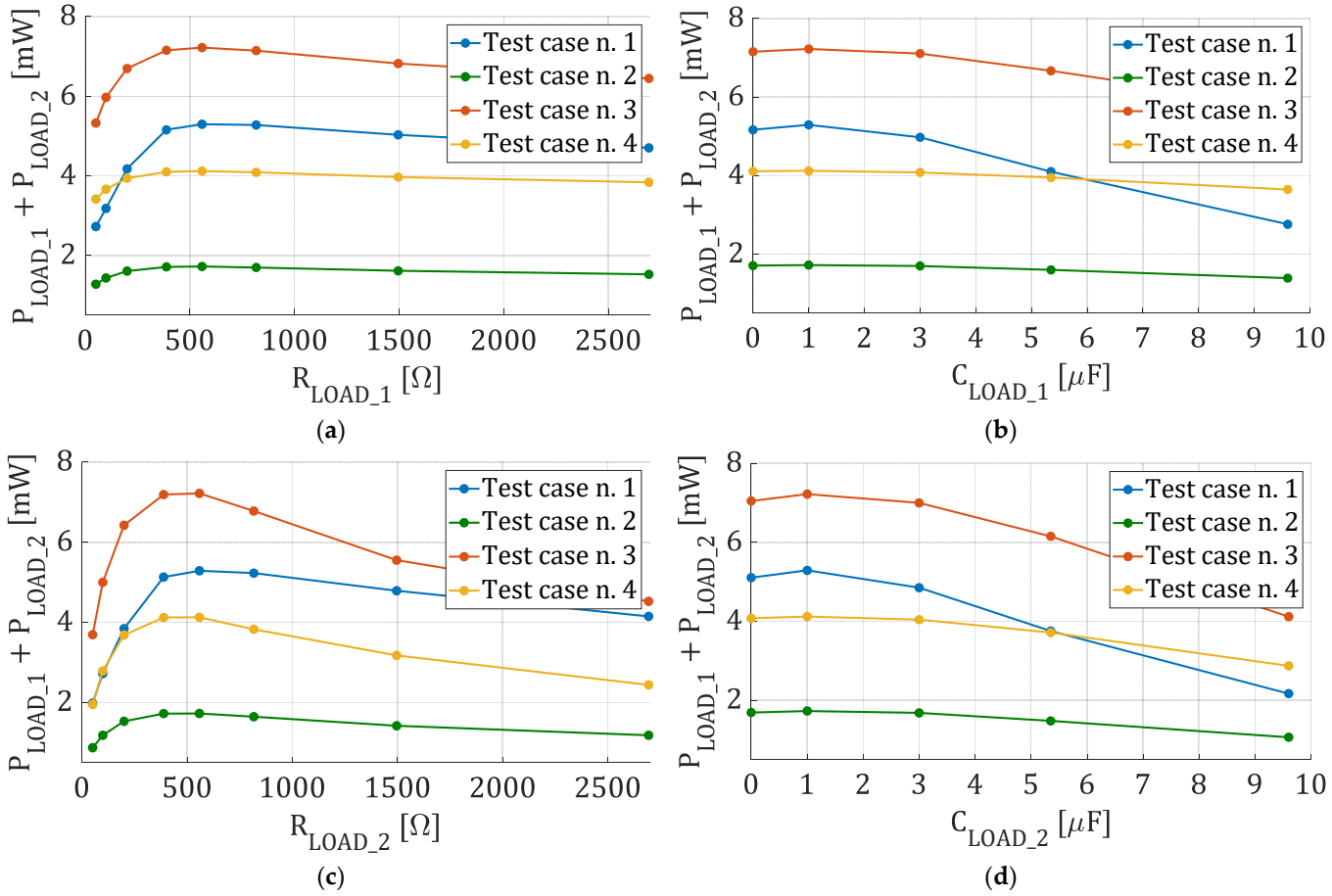

Figure 14. Measured load average power for the double coil circuit in Figure 11a, in the four test cases. (**a**) Power as a function of R_{LOAD_1} for the optimal values of C_{LOAD_1}, R_{LOAD_2} and C_{LOAD_2}. (**b**) Power as a function of C_{LOAD_1} for the optimal values of R_{LOAD_1}, R_{LOAD_2} and C_{LOAD_2}. (**c**) Power as a function of R_{LOAD_2} for the optimal values of C_{LOAD_2}, R_{LOAD_1} and C_{LOAD_1}. (**d**) Power as a function of C_{LOAD_2} for the optimal values of R_{LOAD_2}, R_{LOAD_1} and C_{LOAD_1}.

5. Conclusions

For the first time, the power extraction capability of a double coil electromagnetic harvester was experimentally compared with that of a standard single coil electromagnetic harvester. The validity of the single degree of freedom model used for the comparison was verified by experimental tests on a commercial electromagnetic harvester. The comparison was performed by simulations and by experiments on the electrical circuits modeling the harvester's behavior. The circuits were implemented through electronic components mounted on a solderless breadboard. The experimental results showed that the double coil electromagnetic harvester is able to increase the power delivered to the optimal load for any vibration frequency, but the gain is particularly significant at frequencies lower than the harvester resonance frequency.

The double coil electromagnetic harvester investigated in this paper is characterized by significant advantages with respect to the other techniques proposed in the literature to increase the energy efficiency of electromagnetic harvesters. In particular, the double coil harvester is able to significantly improve the extracted power as in the case of harvester arrays, non-linear harvesters and mechanical tuning techniques. However, its size is smaller than harvester arrays, its complexity is less than that of non-linear harvesters, and it does not need additional actuators as in the case of mechanical tuning techniques. Moreover, the double coil harvester exploits the electrical load matching like the electrical tuning

techniques, but it achieves higher performance than the standard application of an electrical tuning technique.

Author Contributions: Conceptualization, L.C., A.L.S. and M.V.; methodology, L.C., A.L.S. and M.V.; software, L.C., A.L.S. and M.V.; validation, L.C., A.L.S. and M.V.; formal analysis, L.C., A.L.S. and M.V.; investigation, L.C., A.L.S. and M.V.; resources, L.C., A.L.S. and M.V.; data curation, L.C., A.L.S. and M.V.; writing—original draft preparation, L.C., A.L.S. and M.V.; writing—review and editing, L.C., A.L.S. and M.V.; visualization, L.C., A.L.S. and M.V.; supervision, L.C., A.L.S. and M.V.; project administration, L.C., A.L.S. and M.V.; funding acquisition, L.C., A.L.S. and M.V. All authors have read and agreed to the published version of the manuscript.

Funding: This research was partially funded: by the research program "VALERE: VAnviteLli pEr la RicErca" by Università degli Studi della Campania "Luigi Vanvitelli", under grant PE-15/204/E-PASSION, and by the funding program "Valorizzazione di Brevetti tramite il finanziamento di progetti Proof of Concept" by the Italian Ministero per lo Sviluppo Economico (MISE), under grant #NOACRONYM-PoCn1-TEMELEV.

Conflicts of Interest: The authors declare no conflict of interest.

References

1. Delle Femine, A.; Gallo, D.; Landi, C.; Lo Schiavo, A.; Luiso, M. Low power contactless voltage sensor for low voltage power systems. *Sensors* **2019**, *19*, 3513. [CrossRef] [PubMed]
2. Kazmierski, T.J.; Beeby, S. *Energy Harvesting Systems*; Springer: New York, NY, USA, 2011.
3. Newell, D.; Duffy, M. Review of power conversion and energy management for low-power, low-voltage energy harvesting powered wireless sensors. *IEEE Trans. Power Electron.* **2019**, *34*, 9794–9805. [CrossRef]
4. Harb, A. Energy harvesting: State-of-the-art. *Renew. Energy* **2011**, *36*, 2641–2654. [CrossRef]
5. Costanzo, L.; Lin, T.; Lin, W.; Lo Schiavo, A.; Vitelli, M.; Zuo, L. Power electronic interface with an adaptive MPPT technique for train suspension energy harvesters. *IEEE Trans. Industrial Electron.* **2021**, *68*, 8219–8230. [CrossRef]
6. Costanzo, L.; Liu, M.; Lo Schiavo, A.; Vitelli, M.; Zuo, L. Backpack energy harvesting system with maximum power point tracking capability. *IEEE Trans. Ind. Electron.* **2022**, *69*, 506–516. [CrossRef]
7. Cascetta, F.; Lo Schiavo, A.; Minardo, A.; Musto, M.; Rotondo, G.; Calcagni, A. Analysis of the energy extracted by a harvester based on a piezoelectric tile. *Curr. Appl. Phys.* **2018**, *18*, 905–911. [CrossRef]
8. Welcome to the World of Vibrations. Available online: https://www.revibeenergy.com/ (accessed on 15 December 2021).
9. Perpetuum Technology. Available online: https://perpetuum.com/technology/ (accessed on 15 December 2021).
10. Costanzo, L.; Lo Schiavo, A.; Vitelli, M. Active interface for piezoelectric harvesters based on multi-variable maximum power point tracking. *IEEE Trans. Circuits Syst. I Reg. Pap.* **2020**, *67*, 2503–2515. [CrossRef]
11. Costanzo, L.; Lo Schiavo, A.; Vitelli, M. Design guidelines for the perturb and observe technique for electromagnetic vibration energy harvesters feeding bridge rectifiers. *IEEE Trans. Ind. Appl.* **2019**, *55*, 5089–5098. [CrossRef]
12. Brignole, O.; Cavaletti, C.; Maresca, A.; Mazzino, N.; Balato, M.; Buonomo, A.; Costanzo, L.; Giorgio, M.; Langella, R.; Lo Schiavo, A.; et al. Resonant Electromagnetic Vibration Harvesters Feeding Sensor Nodes for Real-Time Diagnostics and Monitoring in Railway Vehicles for Goods Transportation: A Numerical-Experimental Analysis. In Proceedings of the 2016 IEEE International Power Electronics and Motion Control Conference (PEMC 2016), Varna, Bulgaria, 25–30 September 2016; pp. 456–461.
13. Tang, L.; Yang, Y.; Soh, C.K. Toward broadband vibration-based energy harvesting. *J. Intell. Mater. Syst. Struct.* **2010**, *21*, 1867–1897. [CrossRef]
14. Zhu, D.; Tudor, M.J.; Beeby, S.P. Strategies for Increasing the operating frequency range of vibration energy harvesters: A review. *Meas. Sci. Technol.* **2010**, *21*, 1–29. [CrossRef]
15. Andò, B.; Baglio, S.; Bulsara, A.R.; Marletta, V.; Pistorio, A. Experimental and theoretical investigation of a nonlinear vibrational energy harvester. *Procedia Eng.* **2015**, *120*, 1024–1027. [CrossRef]
16. Xie, L.; Du, R. Frequency tuning of a nonlinear electromagnetic energy harvester. *ASME J. Vib. Acoust.* **2013**, *136*, 011010:1–011010:7. [CrossRef]
17. Costanzo, L.; Vitelli, M. Tuning techniques for piezoelectric and electromagnetic vibration energy harvesters. *Energies* **2020**, *13*, 527. [CrossRef]
18. Bowden, J.A.; Burrow, S.G.; Cammarano, A.; Clare, L.R.; Mitcheson, P.D. Switched-mode load impedance synthesis to parametrically tune electromagnetic vibration energy harvesters. *IEEE ASME Trans. Mechatron.* **2015**, *20*, 603–610. [CrossRef]
19. Toh, T.T.; Wright, S.W.; Mitcheson, P.D. Resonant frequency tuning of an industrial vibration energy harvester. *J. Phys. Conf. Ser.* **2014**, *557*, 012128. [CrossRef]
20. Sutrisno, I.W.; Wahied, A.G. A review on frequency tuning methods for piezoelectric energy harvesting systems. *J. Renew. Sustain. Energy* **2012**, *4*, 062703. [CrossRef]
21. Lee, B.C.; Chung, G.S. Frequency tuning design for vibration-driven electromagnetic energy harvester. *IET Renew. Power Gener.* **2015**, *9*, 801–808. [CrossRef]

22. Sun, W.; Jung, J.; Wang, X.Y.; Kim, P.; Seok, J.; Jang, D.Y. Design, simulation, and optimization of a frequency-tunable vibration energy harvester that uses a magnetorheological elastomer. *Adv. Mech. Eng.* **2015**, *7*, 147421:1–147421:6. [CrossRef]
23. Mansour, M.O.; Arafa, M.H.; Megahed, S.M. Resonator with magnetically adjustable natural frequency for vibration energy harvesting. *Sens. Actuators A Phys.* **2010**, *163*, 297–303. [CrossRef]
24. Aboulfotoh, N.A.; Arafa, M.H.; Megahed, S.M. A self-tuning resonator for vibration energy harvesting. *Sens. Actuators A Phys.* **2013**, *201*, 328–334. [CrossRef]
25. Heit, J.; Christensen, D.; Roundy, S. A Vibration Energy Harvesting Structure, Tunable over a Wide Frequency Range Using Minimal Actuation. In Proceedings of the ASME 2013 Conference on Smart Materials, Adaptive Structures and Intelligent Systems (SMASIS 2013), Snowbird, UT, USA, 16–18 September 2013.
26. Eichhorn, C.; Tchagsim, R.; Wilhelm, N.; Woias, P. A smart and self-sufficient frequency tunable vibration energy harvester. *J. Micromech. Microeng.* **2011**, *21*, 104003. [CrossRef]
27. Balato, M.; Costanzo, L.; Lo Schiavo, A.; Vitelli, M. Vibration Energy Harvester, Optimized by electronically Emulated Mechanical Tuning Technique. PCT Application Number PCT/EP2019/056601, International Publication No. WO2019/175413A1, 19 September 2019.
28. Elvin, N.G.; Elvin, A.A. An experimentally validated electromagnetic energy harvester. *J. Sound Vib.* **2011**, *330*, 2314–2324. [CrossRef]